THE ASTRONOMICAL JOURNAL VOLUME 100, NUMBER 6 DECEMBER 1990

ACCURACY OF BINARY STAR SEPARATIONS ESTIMATED FROM INTERFEROMETRIC DATA

M. VIVEKANAND[a),b),c)]
Universities Space Research Association, 600 Maryland Avenue, SW, Suite 303, West Wing, Washington, DC 20024
Received 17 April 1990; revised 18 June 1990

ABSTRACT

This article discusses errors on binary star separations that are estimated by model-fitting visibilities obtained from a two element interferometer. It is shown that the rms error on any component of a binary star's separation in the sky is linearly proportional to the rms noise on the observed visibilities, and linearly proportional to an effective beamwidth for the observation (given by the wavelength divided by an effective length of baseline of the interferometer); it varies inversely with the peak-to-peak variation of the visibility of the binary that depends upon the ratio of intensities of the two stars, and inversely as the square root the total number of observed visibilities. The errors are independent of the binary separation or its orientation in the plane of the sky; this result is not obvious as the model-fitting procedure is essentially nonlinear in the binary star parameters. It is also shown that in principle any visibility dataset can be consistent with more than one binary separation and orientation. This is a consequence of insufficient sampling in the (U,V) plane of the two-dimensional visibility sinusoid. This leads to alternate solutions for the binary separation vector (an effect noted by observers), which may or may not be ruled out on the basis of a minimum χ^2 of model fitting, depending upon the rms noise on the observed visibilities. The alternate solution vectors differ from each other in the two-dimensional binary separation space (i.e., the plane of the sky) by integral multiples of a constant vector that does not depend upon the true vector solution, but only upon the orientation of the interferometer. In other words, the alternate solutions are equally spaced on a straight line in the binary separation space. It is shown that this straight line when projected onto the equatorial plane (i.e., the plane lying at zero declination), is parallel to the projection of the physical baseline onto the same plane. It is possible to think of the alternate solutions as observations of the binary through successive side lobes of an interferometer lying in the equatorial plane, that is actually the projection of the true interferometer (which usually lies in the plane of the ground). The above claims are verified by numerical simulations, as well as by real data from the Mount Wilson optical interferometer.

I. INTRODUCTION

Two element optical interferometers, such as the Mark III at Mount Wilson (Shao *et al.* 1988) and the I2T at CERGA (Labeyrie 1975) have been in operation for some time, and are routinely used to observe stars to estimate their diameters and the separations of binaries in the sky. These instruments typically use two "telescopes" whose separation on the ground is variable. They measure the amplitude of the complex visibility as a function of time, which can be fitted to a three parameter model for binary stars: L_u is the separation between the two stars in right ascension; L_v is the separation in declination, and f is the intensity ratio of the two stars. The best combination of parameters is obtained by minimizing the χ^2 between observed and expected visibilities.

The visibility amplitude I is given by

$$I(t) = \frac{1 + f\cos[\Phi(t)]}{1+f}, \tag{1}$$

where t is the hour angle and Φ is the visibility phase given by

$$\Phi(t) = \frac{2\pi}{\lambda}[U(t)L_u + V(t)L_v], \tag{2}$$

where (U,V) are the components of the projected baseline (i.e., the vector separation between the two telescopes projected onto the plane of the sky), and λ is the wavelength of observation. The visibility amplitude $I(t)$ is the sum of a constant term $1/(1+f)$ and a sinusoid $f\cos[\Phi(t)]/(1+f)$ in the two-dimensional (U,V) space (it is assumed that the binary parameters do not change on timescales of the duration of observations). The visibility phase $\Phi(t)$ refers to the geometric phase of the visibility sinusoid sampled in the (U,V) plane by the instantaneous projection of the physical baseline. It is not the phase of the complex visibility, which is not at all used in this analysis; for want of a better appellation this phrase, although somewhat confusing, has been used throughout this article.

The principle aim of this article is to understand the random and systematic errors associated with L_u and L_v that are estimated by model-fitting Eq. (1) to real data. Section II discusses the rms errors σ_u (on L_u) and σ_v (on L_v) that are expected on account of random noise on the observed visibilities. Section III discusses a systematic error in L_u and L_v that has been noted by observers, that gives rise to alternate solutions for the binary separation parameters L_u and L_v, that is caused by insufficient sampling of the two-dimensional visibility sinusoid $I(t)$.

The above problems have been tackled by the following approach. Consider a visibility dataset $I(t_i)$ observed at specific instants t_i, which implies at specific points $[U(t_i),V(t_i)]$ in the (U,V) plane. One can estimate the change in visibility $\Delta I(t_i)$ at each instant t_i expected by using binary separations that differ by l_u and l_v from the true solution L_u and L_v, respectively. For "small" values of l_u and l_v it is easy to show that $\Delta I(t_i)$ is also a two-dimensional sinusoid in the (U,V) plane [Eq. (11)]. Given this analytic form it is easy to estimate the mean value $\langle \Delta I \rangle$ of $\Delta I(t_i)$ as a function of time t_i, and its second moment $\langle \Delta I^2 \rangle$, which will be called the systematic deviation of the visibility curve [i.e.,

[a)] Naval Research Laboratory, Washington, DC.
[b)] Visiting Associate at California Institute of Technology, Pasadena, CA.
[c)] On leave from Raman Research Institute, Bangalore, India.

 0004-6256/90/062047-14$00.90

the square of the visibility deviation averaged over the duration of observation, elaborated in Eq. (12)]. Under the reasonable assumption made in Sec. II $\langle \Delta I \rangle$ is a small quantity, and $\langle \Delta I^2 \rangle$ is a good estimate of the excess variance expected between the data and Eq. (1), as a function of l_u and l_v; the observed variance will be the sum of $\langle \Delta I^2 \rangle$ and the nominal variance on the visibility data due to random noise. Then one can estimate σ_u and σ_v by the standard statistical criterion that the χ^2 of the model-fitting procedure increases by 1 when $l_u = \sigma_u$ and $l_v = \sigma_v$.

Since $\Delta I(t)$ is a function of two error parameters l_u and l_v, $\langle \Delta I^2 \rangle$ depends not only upon the individual value of l_u and l_v, but also upon their ratio, i.e., the errors on L_u and L_v are correlated. Physically this implies that $\langle \Delta I^2 \rangle$ depends both upon the magnitude $l = \sqrt{l_u^2 + l_v^2}$ and direction of departure from the true solution in the binary separation space. Ideally $\langle \Delta I^2 \rangle$ should vary quadratically with l_u and l_v, and one should derive the equation of the "error ellipse" in this space. Unfortunately it is not easy to derive the equation of the error ellipse analytically. So in this article the following practical approach has been adopted: $\langle \Delta I^2 \rangle$ is estimated as a function of the departure l along two orthogonal directions in the binary separation space. Along one $\langle \Delta I^2 \rangle$ varies least with l, as compared to any other direction; this would obviously yield the largest l consistent with the data, and should correspond to estimating the error along the major axis of the error ellipse. Along the other $\langle \Delta I^2 \rangle$ varies most with l, and should correspond to estimating the error along the minor axis of the error ellipse. Thus two sets of formulas are derived for σ_u and σ_v, for the two directions along which $\langle \Delta I^2 \rangle$ varies the most and the least, respectively, with the departure l from the true solution. Both have to be used judiciously to estimate the final errors on the binary parameters. Because of the above approximations these expressions for σ_u and σ_v are expected to predict only ball-park estimates of the true errors.

In Sec. II analytic expressions are derived for σ_u and σ_v that predict the observed errors to within a factor of 2, on the average. They turn out to be independent of L_u and L_v—a happy surprise. It is shown that σ_u and σ_v are directly proportional to an effective beamwidth for the observation given by $\lambda / d_{\rm eff}$, where $d_{\rm eff}$ is an effective length of baseline for the duration of the observation, which in most cases is approximately equal to the length of the physical baseline projected onto the equatorial plane [Eq. (20); see also Eqs. (19) and (22) for special cases]. They scale directly with the rms noise on the visibility measurements. They vary inversely with the total variation of the expected visibility, which depends upon f. Finally they vary inversely with the square root of the number of observed visibilities. Table I shows the agreement between the formulas of Sec. II and some observing situations that have been chosen at random.

Section III discusses the systematic errors on L_u and L_v due to insufficient sampling of $I(t)$ in the (U,V) plane. As mentioned earlier I varies sinusoidally over the two-dimensional (U,V) plane. Let the two stars of a binary lie along the direction **a** in the plane of the sky [also the (U,V) plane, see Fig. 1]. They will "produce" visibility fringes in this plane (solid lines in Fig. 1) that are sampled by the projected baseline vector which moves along the arc of an ellipse as time progresses [details of this ellipse can be found in Thompson *et al.* (1986)]. Obtaining the true L_u and L_v implies obtaining the period of these visibility fringes and their orientation in the (U,V) plane. In principle this can be done without bias if one is allowed to sample $I(t)$ arbitrarily in the (U,V) plane. However, in a practical situation one is limited to a finite duration of observation, during which the physical baseline traces only a finite segment of an ellipse, and one samples $I(t)$ along this curve. Now it is obvious that the locus of the projected baseline must satisfy certain criterion if one is to recover all information unambiguously. For example, if the locus were a straight line instead of an ellipse, it is clear that one would obtain an $I(t)$ that is perfectly sinusoidal in time; this could imply an infinite number of two-dimensional solutions, each with a slightly different orientation in the (U,V) plane but with a correspondingly consistent period. To obtain the complete information one would have to sample $I(t)$ along two orthogonal directions in the (U,V) plane. The ellipse can effectively do that provided the duration of the observation is sufficiently large. Unfortunately, this is not often the case. A finite duration of observation can be

TABLE I. Comparison of observed and expected σ_u and σ_v in four random examples. The first column contains the parameters of the simulated data: the latitude of the interferometer Λ, the declination of the binary star δ, physical baseline components X, Y, and Z, components of the binary separation L_u and L_v, intensity ratio f, the wavelength of the observation λ, and the total number of observed visibilities N. The next two columns contain the expected and the observed σ_u and σ_v, respectively, for a Gaussian random noise of rms value $\sigma_{\rm obs} = 0.05$ on the simulated visibilities. The next pair of columns has the same information for $\sigma_{\rm obs} = 0.15$, and the last pair of columns has information for $\sigma_{\rm obs} = 0.30$. The expected σ_u and σ_v are computed from Eqs. (18) and (21), while the observed ones are estimated from the simulated data by the criterion that the χ^2 increase by 1 at these offsets. Even at declinations as low as 10° σ_u and σ_v are predicted well by Eqs. (18) and (21).

Parameters of simulation	$\sigma_{\rm obs} = 0.05$		$\sigma_{\rm obs} = 0.15$		$\sigma_{\rm obs} = 0.30$	
$\Lambda = 35°$; $\delta = 45°$; $\lambda = 0.4\,\mu$; $N = 56$;	exp	obs	exp	obs	exp	obs
$X = 5$ m; $Y = 10$ m; $Z = 0$ m;	$\sigma_u = 0.035$	$\sigma_u = 0.035$	$\sigma_u = 0.105$	$\sigma_u = 0.113$	$\sigma_u = 0.210$	$\sigma_u = 0.195$
$L_u = -20.479$ mas; $L_v = 14.339$ mas; $f = 0.65$	$\sigma_v = 0.044$	$\sigma_v = 0.044$	$\sigma_v = 0.132$	$\sigma_v = 0.141$	$\sigma_v = 0.264$	$\sigma_v = 0.243$
$\Lambda = 45°$; $\delta = 75°$; $\lambda = 0.8\,\mu$; $N = 65$;	exp	obs	exp	obs	exp	obs
$X = -2.5$ m; $Y = 4.3$ m; $Z = 0$ m;	$\sigma_u = 0.136$	$\sigma_u = 0.122$	$\sigma_u = 0.408$	$\sigma_u = 0.373$	$\sigma_u = 0.816$	$\sigma_u = 0.788$
$L_u = -31.466$ mas; $L_v = -38.857$ mas; $f = 1.0$	$\sigma_v = 0.111$	$\sigma_v = 0.100$	$\sigma_v = 0.333$	$\sigma_v = 0.304$	$\sigma_v = 0.666$	$\sigma_v = 0.647$
$\Lambda = 75°$; $\delta = 20°$; $\lambda = 0.6\,\mu$; $N = 69$;	exp	obs	exp	obs	exp	obs
$X = 15$ m; $Y = -7.7$ m; $Z = 1$ m;	$\sigma_u = 0.025$	$\sigma_u = 0.023$	$\sigma_u = 0.075$	$\sigma_u = 0.064$	$\sigma_u = 0.150$	$\sigma_u = 0.125$
$L_u = 12.287$ mas; $L_v = -8.604$ mas; $f = 0.8$	$\sigma_v = 0.082$	$\sigma_v = 0.085$	$\sigma_v = 0.246$	$\sigma_v = 0.220$	$\sigma_v = 0.492$	$\sigma_v = 0.457$
$\Lambda = -30°$; $\delta = 10°$; $\lambda = 1.0\,\mu$; $N = 68$;	exp	obs	exp	obs	exp	obs
$X = -7.5$ m; $Y = -10$ m; $Z = 2$ m;	$\sigma_u = 0.052$	$\sigma_u = 0.050$	$\sigma_u = 0.156$	$\sigma_u = 0.142$	$\sigma_u = 0.312$	$\sigma_u = 0.299$
$L_u = 64.952$ mas; $L_v = 37.5$ mas; $f = 0.55$	$\sigma_v = 0.131$	$\sigma_v = 0.127$	$\sigma_v = 0.393$	$\sigma_v = 0.359$	$\sigma_v = 0.686$	$\sigma_v = 0.756$

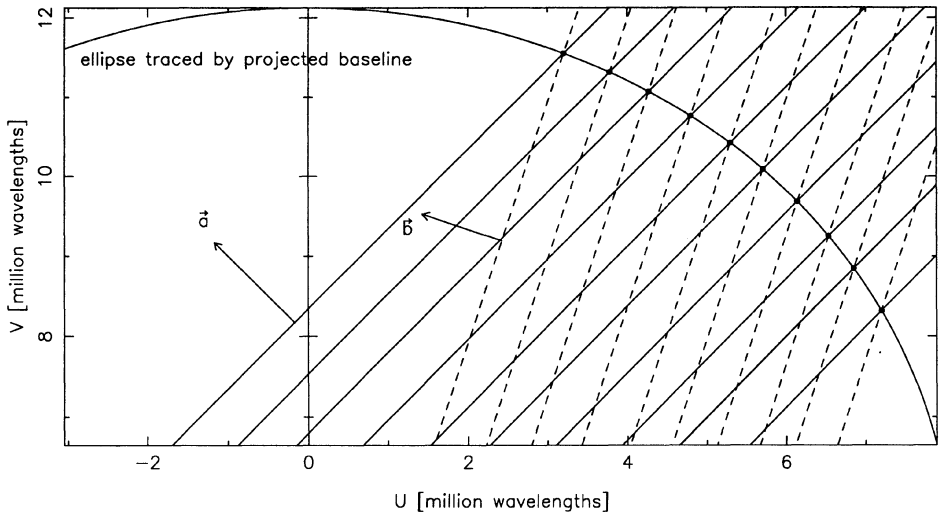

FIG. 1. Physical explanation of multiple solutions. **a** is the direction of orientation of a binary separation in the plane of the sky or the (U,V) plane. It is orthogonal to the solid lines which represent the maxima of the resulting visibility fringes. They are sampled by the projected baseline, which moves along an ellipse as time progresses. If these visibility fringes were observed only at the maxima (shown by dots), then the data would also be consistent with the fringes represented by the dashed lines, which would imply the binary orientation **c**.

partly compensated by a higher sampling rate of visibility in the (U,V) plane; this is also not always feasible in a practical situation. This is how a finite visibility dataset can be fit to more than one solution for the binary separation.

Consider the extreme case in Fig. 1 where the visibility was sampled only at the peaks of the two-dimensional fringes (marked by dots in Fig. 1). Then one could fit the solution **b** also to the same data, whose fringes are the dashed lines in Fig. 1. If the data is well sampled, or if the noise on the visibilities is low, then **c** can be ruled out on the basis of χ^2 alone.

Thus Sec. III discusses the uniqueness of the solution to Eq. (1), due to the finite duration of the observation and finite sampling rate of the visibility. The question addressed is, are there other binary separations and orientations, distinct from each other, at which $\langle \Delta I^2 \rangle$ has a minimum comparable to that at the true solution, due to a combination of large measurement or calibration errors on the visibilities, finite duration of the observation, and insufficient sampling? The answer is yes, and Sec. III develops the mathematical basis of this phenomenon.

The analytic approach is an extension of that described above. As before one considers changes in L_u and L_v by l_u and l_v, respectively, and looks for minima in $\langle \Delta I^2 \rangle$ that are comparable to the true minima. However, now l_u and l_v are much larger than the corresponding rms errors σ_u and σ_v that were discussed above. Let the corresponding change in visibility phase be represented by $\phi(t)$. It is shown in Sec. III that the binary separations can be changed from the true values by l_u and l_v, that are much larger than σ_u and σ_v, in such a manner that the change in visibility phase $\phi(t)$ [Eq. (9)] at each hour angle t is "small," and it remains small for the largest possible duration of time. Then the two visibility curves will look "similar," on the whole. These conditions are more easily satisfied if the duration of observation is not greater than $\approx$6–9 hr, which is often the practical situation. Then, depending upon the rms noise on the observed visibilities, it may not be possible to choose between the two solutions based on χ^2 alone.

In principle the change in visibility phase $\phi(t)$ is proportional to $l = \sqrt{l_u^2 + \sin^2 \delta l_v^2}$ (where δ is the declination of the binary); i.e., $\phi(t)$ increases approximately linearly with departure from the true solution. The trick is to let l_u and l_v increase sufficiently so that $\phi(t)$ is of the order of 2π, which amount drops out of Eq. (1)! Then only the residual phase [i.e., $\phi(t)$ modulo 2π] is effective in Eq. (1), which can be a small quantity. However, this condition by itself is not sufficient to mimic the true solution, since $\phi(t)$ may be different from 2π at other hour angles. Therefore one has to change L_u and L_v along the right direction in the binary separation space (say Θ_a), so that $\phi(t)$ will remain "small" over a significant fraction of the duration of observation, satisfying both the conditions above.

In Sec. III analytic expressions are derived for the direction Θ_a in the binary separation space along which the alternate solutions lie, as well as for the separation between the alternate solutions. It is shown that alternate solutions also lie along the direction $\Theta_a + 180°$. This direction, when projected onto the equatorial plane, is parallel to the projection of the physical baseline onto the same plane. This is like observing the binary through sidelobes of an interferometer that is the projection of the actual interferometer onto the equatorial plane. The alternate solutions are equally spaced in the plane of the sky, just as the sidelobes are equally spaced in angle in the sky. Figure 4 illustrates the alternate solutions of the first example in Table I, and Table II compares the observed and expected parameters of the alternate solutions of all four examples of Table I.

Section IV discusses the assumptions underlying the above results, and their implications and limitations. It concludes with a comparison of the above theory with real data from Mount Wilson optical interferometer. Table III compares the σ_u and σ_v expected from Sec. II with the observed errors on the separation of the spectroscopic binary α Andromeda. The expected values are systematically lower by a factor of $\approx$2 (on the average) than the observed values. This is partly due to an approximation made in Secs. II*a* and II*b* which enabled one to obtain analytically simple expressions for σ_u and σ_v, as well as systematic effects in the data, as discussed in Sec. IV. Figure 5 illustrates the alternate solutions found in one night's observation of α Andromeda.

II. rms ERRORS ON L_u AND L_v

Equation (2) can be rewritten as

$$\Phi(t) = \frac{2\pi}{\lambda}[U(t)L_u + V(t)L_v]$$
$$= \frac{2\pi}{\lambda}[X\cos t - (Y\sin\Lambda - Z\cos\Lambda)\sin t]L_u + \frac{2\pi}{\lambda}[X\sin\delta\sin t + (Y\sin\Lambda - Z\cos\Lambda)$$
$$\times\sin\delta\cos t + (Y\cos\Lambda + Z\sin\Lambda)\cos\delta]L_v$$
$$= D\cos(t-\Theta) + C \qquad (3)$$

where

$$D = (2\pi/\lambda)\sqrt{X^2 + (Y\sin\Lambda - Z\cos\Lambda)^2}$$
$$\times\sqrt{L_u^2 + \sin^2\delta L_v^2}$$
$$\cos\Theta = (2\pi/\lambda D)[XL_u + (Y\sin\Lambda - Z\cos\Lambda)\sin\delta L_v]$$
$$\sin\Theta = (2\pi/\lambda D)[X\sin\delta L_v - (Y\sin\Lambda - Z\cos\Lambda)L_u]$$
$$C = (2\pi/\lambda)(Y\cos\Lambda + Z\sin\Lambda)\cos\delta L_v \qquad (4)$$

X, Y, and Z are the components of the physical baseline [X points east, Y points north, and Z points along the local meridian; see Thompson *et al.* (1986)], and Λ is the geographical latitude of the interferometer. The visibility phase Φ varies sinusoidally with the hour angle t. Its amplitude D and its phase Θ* have a simple physical interpretation. Consider the projection of the physical baseline and the binary separation onto the equatorial plane [Fig. 2(b)]. The plane of the ground is inclined to it at $90° - \Lambda$ and the plane of the sky is inclined at $90° - \delta$ [Fig. (2a)]. Let the unit vectors **x** and **y** define an orthogonal coordinate system in Fig. 2(b); let **y** lie along the projection of the local meridian, pointing towards "north," and let **x** point towards "east." Then

$$\mathbf{R} = X\mathbf{x} + (Y\sin\Lambda - Z\cos\Lambda)\mathbf{y} \qquad (5)$$

is the projection of the physical baseline onto the equatorial plane, while the projection of the binary separation is

$$\mathbf{r} = L_u\mathbf{x} + \sin\delta L_v\mathbf{y} \qquad (6)$$

Let $R = \sqrt{X^2 + (Y\sin\Lambda - Z\cos\Lambda)^2}$ and $r = \sqrt{L_u^2 + \sin^2\delta L_v^2}$ be the lengths of the corresponding vectors (note that R has units of length while r has units of radians). Then

$$D = \frac{2\pi}{\lambda}|\mathbf{R}||\mathbf{r}| = \frac{2\pi}{\lambda}Rr \qquad (7)$$

is proportional to the product of the two lengths, while

$$\Theta = \arccos\left(\frac{\mathbf{R}\cdot\mathbf{r}}{|\mathbf{R}||\mathbf{r}|}\right) \qquad (8)$$

is the angle between the two vectors in the equatorial plane [Fig. 2(b)]. C is the constant part of Φ that arises due to the projections of the binary separation ($\cos\delta L_v$) and the physical baseline ($Y\cos\Lambda + Z\sin\Lambda$) along the rotation axis of Earth, which have no time dependence due to Earth rotation. Thus the seven parameters of the problem ($\delta, \Lambda, X, Y, Z, L_u, L_v$) have been reduced to three (D,Θ, and C) by considering the problem in terms of projections in the equatorial plane and along the rotation axis of Earth.

Since Φ is linear in the parameters L_u and L_v, a change in them by l_u and l_v causes $\Phi(t)$ to change by $\phi(t)$

$$\phi(t) = \frac{2\pi}{\lambda}[U(t)l_u + V(t)l_v]$$
$$= d\cos(t-\theta) + c, \qquad (9)$$

where

$$d = \frac{2\pi}{\lambda}\sqrt{X^2 + (Y\sin\Lambda - Z\cos\Lambda)^2}\sqrt{l_u^2 + \sin^2\delta l_v^2}$$
$$= \frac{2\pi}{\lambda}Rl,$$
$$\cos\theta = \frac{1}{Rl}[Xl_u + (Y\sin\Lambda - Z\cos\Lambda)\sin\delta l_v],$$
$$\sin\theta = \frac{1}{Rl}[X\sin\delta l_v - (Y\sin\Lambda - Z\cos\Lambda)l_u],$$
$$c = \frac{2\pi}{\lambda}(Y\cos\Lambda + Z\sin\Lambda)\cos\delta l_v, \qquad (10)$$

which is also a sinusoid (Fig. 3). d, θ, and c are the same as D, Θ, and C of Eq. (4), with L_u and L_v replaced by l_u and l_v,

TABLE II. Properties of the alternate solutions of the examples in Table I, arranged sequentially in the same order as in Table I. For each example the first two pairs of alternate solutions are considered. The expected coordinate offsets l_u and l_v of the alternate solutions, with respect to the true solution L_u and L_v, are shown in columns 2 and 3; they are estimated using Eqs. (23) and (25). Column 4 contains the expected rms systematic deviation $\sqrt{\langle\Delta I^2\rangle_a}$ estimated from Eq. (27), while the last column shows the observed rms deviation of the visibility curves from the simulated data. In principle this also contains the rms noise σ_{obs} on the simulated data, added in quadrature to $\sqrt{\langle\Delta I^2\rangle_a}$; however $\sigma_{obs} = 0.05$ has been used in this table, which is much smaller than any of these $\sqrt{\langle\Delta I^2\rangle_a}$, so that its effect in column 5 can be ignored, except in example 4. At larger σ_{obs} the alternate solutions are expected to become more prominent. Except in example 3, the alternate solutions occur almost exactly at the predicted offsets in columns 2 and 3. In example 3 the first alternate solution occurs $\approx$0.5 mas away from the predicted value. The expected $\langle\Delta I^2\rangle_a$ in the last example is very small because the duration of observation Δt is very small, due to the very low declination of the binary; the 0.05 in the third column is actually σ_{obs}, which is the minimum observable rms deviation.

	l_u mas	sin δl_v mas	$\sqrt{\langle\Delta I^2\rangle_a}$ (exp)	$\sqrt{\langle\Delta I^2\rangle_a}$ (obs)
1	+ 3.965	+ 4.501	0.13	0.21
	− 3.965	− 4.501	0.13	0.22
	+ 7.930	+ 9.002	0.27	0.33
	− 7.930	− 9.002	0.27	0.36
2	− 22.320	+ 28.320	0.48	0.39
	+ 22.320	− 28.320	0.48	0.37
	− 44.640	+ 56.640	0.96	0.48
	+ 44.640	− 56.640	0.96	0.45
3	+ 5.998	− 3.211	0.51	0.40
	− 5.998	+ 3.211	0.51	0.41
	+ 11.996	− 6.442	1.02	0.42
	− 11.996	+ 6.442	1.02	0.46
4	− 13.268	− 5.998	0.05	0.16
	+ 13.268	+ 5.998	0.05	0.16
	− 27.256	− 11.976	0.11	0.31
	+ 27.256	+ 11.976	0.11	0.29

*Θ is the phase of the sinusoid that represents the variation of the visibility phase $\Phi(t)$ as a function of hour angle t.

TABLE III. Comparison of observed and expected σ_u and σ_v for four different observations of the binary star α Andromeda. The dates of the observations are shown in column 1; the X, Y, and Z components of the physical baseline in columns 2, 3, and 4; the central hour angle t_0 and the total duration of observation Δt in columns 5 and 6. Columns 7 and 8 contain the effective beamwidths λ/d_{u2} and λ/d_{v1} along the two axis. Column 9 contains the total number of visibilities observed that night, and column 10 contains the observed rms noise σ_{obs} on the visibility squared data. Columns 11 and 12 show the expected and observed σ_u, respectively, while columns 13 and 14 contain the expected and observed σ_v. Table III (a) shows data obtained at a wavelength of 0.8 μm and Table III (b) has data obtained at 0.55 μm. α Andromeda has $f = 0.18$ and $\delta \approx 29.04°$. Note that the expression $(1+f)/f$ in Eq. (18) and (21) is replaced by $(1+f)^2/2f$ since one is working with the visibility squared data.

DATE	X (m)	Y (m)	Z (m)	t_0 (hr)	Δt (hr)	λ/d_{u2} (mas)	λ/d_{v1} (mas)	N	σ_{obs}	$\sigma_u\|_{exp}$ (mas)	$\sigma_u\|_{obs}$ (mas)	$\sigma_v\|_{exp}$ (mas)	$\sigma_v\|_{obs}$ (mas)
8-31-1989	0.2	31.5	0	−0.5	7.0	10.709	1.865	34	0.016	0.04	0.10	0.01	0.03
9-02-1989	0.2	31.5	0	−0.3	7.0	11.980	1.865	19	0.019	0.06	0.08	0.01	0.03
9-09-1989	0.2	23.6	0	−0.05	7.5	16.831	2.508	22	0.023	0.10	0.14	0.02	0.05
9-14-1989	0.1	8.2	0	−0.45	7.1	45.725	7.196	16	0.030	0.42	0.83	0.06	0.24

DATE	X (m)	Y (m)	Z (m)	t_0 (hr)	Δt (hr)	λ/d_{u2} (mas)	λ/d_{v2} (mas)	N	σ_{obs}	$\sigma_u\|_{exp}$ (mas)	$\sigma_u\|_{obs}$ (mas)	$\sigma_v\|_{exp}$ (mas)	$\sigma_v\|_{obs}$ (mas)
8-31-1989	0.2	31.5	0	−0.5	7.0	7.363	1.282	34	0.025	0.04	0.06	0.01	0.02
9-02-1989	0.2	31.5	0	−0.3	7.0	8.263	1.282	19	0.025	0.06	0.06	0.01	0.02
9-09-1989	0.2	23.6	0	−0.05	7.5	11.572	1.724	22	0.049	0.15	0.17	0.02	0.05
9-14-1989	0.1	8.2	0	−0.45	7.1	31.436	4.946	16	0.046	0.44	0.63	0.07	0.21

respectively, since $\phi(t)$ is the same as $\Phi(t)$ of Eq. (3) with exactly the same substitutions. l is the length of the vector $\Delta\mathbf{r} = l_u\mathbf{x} + \sin\delta l_v\mathbf{y}$ which is the difference between two solutions of the binary separation, projected onto the equatorial plane; θ is the angle between the vectors $\mathbf{R}$ and $\Delta\mathbf{r}$. For small values of l_u and l_v, and therefore for small values of $\phi(t)$, the change in visibility at any hour angle can be approximated by

$$\Delta I(t) \approx -\left(\frac{f}{1+f}\right)\sin[\Phi(t)]\phi(t). \tag{11}$$

Let the binary be observed from hour angles t_1 to t_2. Then the mean value of ΔI and its second moment can be defined as

$$\langle \Delta I \rangle = \frac{1}{t_2 - t_1}\int_{t_1}^{t_2} \Delta I(t)dt,$$
$$\langle \Delta I^2 \rangle = \frac{1}{t_2 - t_1}\int_{t_1}^{t_2} \Delta I^2(t)dt. \tag{12}$$

Under the reasonable assumption that the visibility $I(t)$ goes through at least one cycle of variation from t_1 to t_2, $\langle \Delta I \rangle$ is a negligible quantity, since $\Phi(t)$ varies much faster than $\phi(t)$, and the second moment is given by

$$\langle \Delta I^2 \rangle = \left(\frac{f}{1+f}\right)^2 \frac{1}{t_2 - t_1}\int_{t_1}^{t_2} \frac{\phi^2(t)}{2}dt, \tag{13}$$

which we will call the *systematic variance* of the visibility curve in the hour angle range $t_2 - t_1$, due to change in binary separation of l_u and l_v.

Ideally the contour of constant $\langle \Delta I^2 \rangle$ is an ellipse in the L_u, L_v space, and one should be able to derive analytic formulas for the correlated errors σ_u and σ_v. However, the mathematics is not simple, so we will derive expressions for σ_u and σ_v along that direction in the L_u, L_v space along which $\langle \Delta I^2 \rangle$ varies slowest with the departure l from the true solution. This would yield the largest values of σ_u and

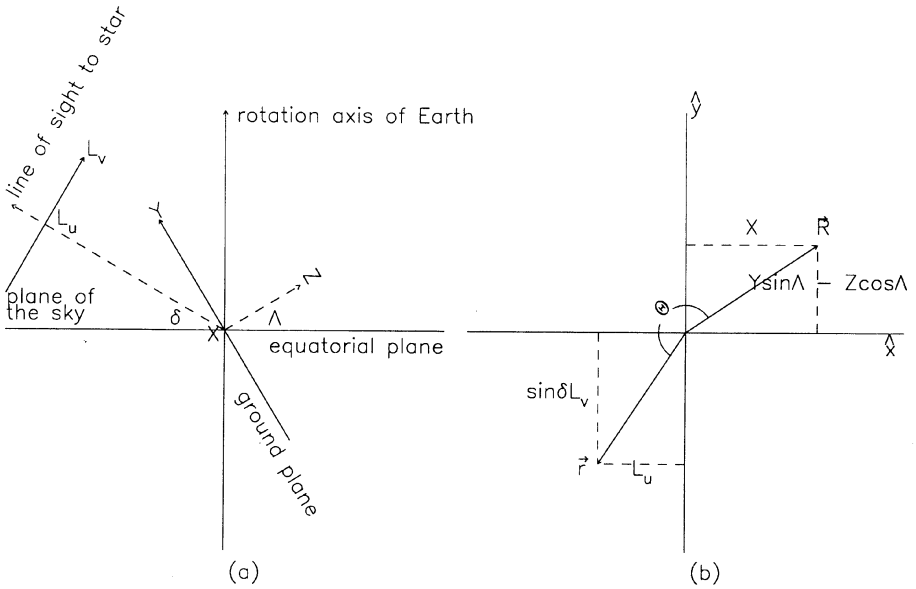

FIG. 2. Geometry of the problem. (a) The local zenith Z is inclined at angle Λ to the equatorial plane, while the line of sight to the binary is inclined at angle δ. X and Y are the components of the physical baseline in the plane of the ground. L_u and L_v are the components of the binary separation the plane of the sky (X and L_u point down the figure). (b) Projection onto the equatorial plane of the physical baseline $\mathbf{R}$ and the binary separation $\mathbf{r}$. X and L_u are projected unmodified as they are parallel to this plane to begin with. It is obvious how Y, Z, and L_v are projected. Θ is the angle between $\mathbf{R}$ and $\mathbf{r}$ measured counter-clockwise.

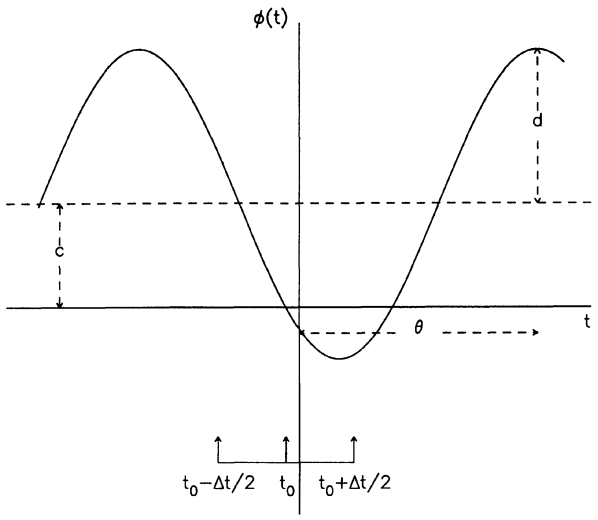

FIG. 3. Schematic of the sinusoidal phase error $\phi(t)$ as a function of the hour angle t, for change in binary separation of l_u and l_v. Its amplitude d, phase θ, and average value c are defined in terms of l_u and l_v in Eq. (10). For an observing session of duration Δt centered at t_0, the allowed l_u and l_v consistent with the data are such that $\phi(t_0)\approx 0$. Then the duration Δt encompasses the smallest possible absolute values of ϕ, which would yield the minimum $\langle \Delta I^2\rangle$. Conversely, for an allowed $\langle \Delta I^2\rangle$ consistent with the data, one would obtain the largest possible errors. When $t_0\approx\theta$, the duration of observation encompasses the largest possible absolute values of ϕ. Moreover the total range of change of ϕ in this time is least.

σ_v consistent with the data, which would also correspond to the errors estimated using the major axis of the error ellipse. In some cases σ_u and σ_v are also determined by the rate of change of $\langle \Delta I^2\rangle$ along the orthogonal direction in the L_u and L_v space; This is obviously that direction along with $\langle \Delta I^2\rangle$ varies fastest, and is equivalent to estimating errors using the minor axis of the error ellipse.

For a given departure of $l=\sqrt{l_u^2+\sin^2\delta l_v^2}$ in the binary separation space, along the direction specified by θ, the components l_u and l_v can be obtained from Eq. (10)

$$l_u=\frac{l\,[X\cos\theta-(Y\sin\Lambda-Z\cos\Lambda)\sin\theta\,]}{\sqrt{X^2+(Y\sin\Lambda-Z\cos\Lambda)^2}}$$

$$=\frac{l}{R}[X\cos\theta-(Y\sin\Lambda-Z\cos\Lambda)\sin\theta\,],$$

$$\sin\delta l_v=\frac{l\,[X\sin\theta+(Y\sin\Lambda-Z\cos\Lambda)\cos\theta\,]}{\sqrt{X^2+(Y\sin\Lambda-Z\cos\Lambda)^2}}$$

$$=\frac{l}{R}[X\sin\theta+(Y\sin\Lambda-Z\cos\Lambda)\cos\theta\,]. \tag{14}$$

Equation (14) is not useful for declinations around 0° as $\sin\delta\approx 0$. In this limit the plane of the sky is vertical to the equatorial plane [see Fig. 2(a)], and L_v has no component in the equatorial plane, and projects only along the rotation axis of Earth. Section II c discusses this special case.

Let the total duration of observation be $\approx$6–9 hr, which is a typical situation practically. This would imply that the duration of observation includes about a quarter cycle of ϕ in Fig. 3. Let $\Delta t=t_2-t_1$ be the range of observed hour angle, and let t_0 be the center of this range.

a) Largest Errors, $t_0-\theta\approx\pm 90°, \pm 270°,\ldots$

From Fig. 3 it is clear that $\langle \Delta I^2\rangle$ will be least when $\phi(t_0)\approx 0$, i.e., when the observed hour angle range is centered at $t_0-\theta\approx\arccos(-c/d)$. Then the observed range of hour angle includes the smallest possible values of $\phi(t)$. At the true solution both l_u and l_v, and therefore c and d, are zero. As l_u and l_v increase, so do c and d. From Eq. (10) it is reasonable to expect d to increase faster than c except for the cases where δ and Λ are small; this requires that the physical baseline and the binary separation have much larger projections in the equatorial plane, than along the rotation axis of Earth. In this subsection it will be assumed that $d\gg c$, since it is then possible to derive analytically simple expressions for σ_u and σ_v. Later it will be argued that the same applies for the case $d\ll c$. Only in the intermediate case $d\approx c$ is it difficult to obtain simple analytically expressions for the effective baseline length $d_{\rm eff}$; this, however, does not change the qualitative nature of the errors.

So to obtain the largest errors one has to change l_u and $\sin\delta l_v$ such that θ satisfies the constraint $t_o-\theta\approx\pm(2n+1)\pi/2, n=0,1,2$, etc. Let $t'=t-t_0$ be the hour angle measured with respect to the central hour angle t_0. By using this and Eqs. (10) and (14) in Eq. (9) one obtains

$$\phi(t')=\pm(-1)^n(2\pi/\lambda)Rl(\sin t'+k_1), \tag{15}$$

where

$$k_1=\frac{(Y\cos\Lambda+Z\sin\Lambda)\,[X\cos t_0-(Y\sin\Lambda-Z\cos\Lambda)\sin t_0\,]}{\tan\delta R^2}. \tag{16}$$

The change in visibility phase ϕ is directly proportional to the departure l from the solution:

$$\Rightarrow\langle\Delta I^2\rangle=\frac{1}{2}\left(\frac{f}{1+f}\right)^2\left(\frac{2\pi}{\lambda}\right)^2R^2l^2\frac{1}{\Delta t}\times\int_{-\frac{\Delta t}{2}}^{+\frac{\Delta t}{2}}(\sin t'+k_1)^2dt'$$

$$=\left(\frac{\pi}{\lambda}\right)^2\left(\frac{f}{1+f}\right)^2R^2l^2\left(1+2k_1^2-\frac{\sin\Delta t}{\Delta t}\right). \tag{17}$$

Let σ_u and σ_v be defined such that at $L_u+\sigma_u$ and $L_v+\sigma_v$ in the parameter space, the systematic variance $\langle \Delta I^2\rangle$ equals $\sigma_{\rm obs}^2/N$, where $\sigma_{\rm obs}^2$ is the variance between the observed visibilities and expected visibilities at the true solution L_u and L_v, and N is the number of observations. This criterion implies that the minimum χ^2 of the fit increases by 1 at $L_u+\sigma_u$ and $L_v+\sigma_v$. Then Eq. (17) will give the distance l one has to move in the parameter space, in the direction characterized by $\theta=t_0\pm(2n+1)\pi/2$, so that the χ^2 increases by 1. Substituting this in Eq. (14), one obtains

$$\sigma_u = \frac{1}{\pi}\frac{\lambda}{d_{u_1}}\sqrt{\frac{1}{N}\left(\frac{1+f}{f}\right)}\sigma_{\rm obs},$$
$$\sigma_v = \frac{1}{\pi}\frac{\lambda}{d_{v1}}\sqrt{\frac{1}{N}\left(\frac{1+f}{f}\right)}\sigma_{\rm obs}, \qquad (18)$$

where

$$\frac{1}{d_{ul}} = -\frac{[X\sin t_0 + (Y\sin\Lambda - Z\cos\Lambda)\cos t_0]}{R^2} \times \frac{1}{\sqrt{1+2k_1^2 - \frac{\sin\Delta t}{\Delta t}}},$$
$$\frac{1}{d_{v1}} = +\frac{[X\cos t_0 - (Y\sin\Lambda - Z\cos\Lambda)\sin t_0]}{R^2} \times \frac{1}{\sqrt{1+2k_1^2 - \frac{\sin\Delta t}{\Delta t}}}, \qquad (19)$$

d_{u1} and d_{v1} have units of length and can be considered to be the effective lengths of baselines along the L_u and L_v axis. σ_u and σ_v are signed quantities because they specify a direction in the L_u,L_v space; it is understood that their absolute values are to be taken for the rms errors on the binary separation.

σ_u and σ_v are directly proportional to the *effective beam widths* λ/d_{u1} and λ/d_{v1} along the respective axis. They scale inversely as the total range of visibility variation $2f/(1+f)$, which is reasonable since it represents the operative part of the visibility curve; the mean visibility of the data is not relevant to the model-fitting procedure. They scale linearly with the rms noise on the visibilities $\sigma_{\rm obs}$, and inversely with the square root of the total number of observations which is intuitively obvious. They decrease with increasing duration of observation, which is also reasonable. Finally they are independent of the parameters L_u and L_v, a result that is not intuitively obvious.

d_{u1} and d_{v1} can be better understood by forming the quantity

$$\frac{1}{d_{\rm eff}} = \left(\frac{1}{d_{u1}^2} + \frac{1}{d_{v1}^2}\right)^{1/2} = \frac{1}{R}\frac{1}{\sqrt{1+2k_1^2 - \frac{\sin\Delta t}{\Delta t}}} \approx \frac{1}{R}\frac{1}{\sqrt{1+2/\tan^2\delta}}, \qquad (20)$$

where Δt is assumed to be sufficiently large, and k_1 is approximated to $1/\tan\delta$, which is reasonable for most Λ. Thus for most declinations $d_{\rm eff}$ is of the order of the length R of the projection of the physical baseline onto the equatorial plane. d_{u1} and d_{v1} are the components of $d_{\rm eff}$ along the L_u and L_v axis.

Equation (18) is only partly useful when the direction of motion in the L_u,L_v space is close to either the L_u or the L_v axis. Then one of the errors σ_u and σ_v is computed to be ≈ 0, which does not mean that the error along that axis is negligible. This occurs because σ_u and σ_v together also represent a direction along which $\langle\Delta I^2\rangle$ changes at a certain rate with the departure l; that direction can very well be along one of the axis L_u or L_v. In that case one has to evaluate σ_u and σ_u along a direction *perpendicular* to the previous direction in the L_u and L_v space.

b) Minimum Errors, $t_0 - \theta \approx 0°, \pm 180°,\ldots$

To begin with, it is assumed that $d \gg c$, as in the previous section. Then from Fig. 3 it is obvious that ϕ has a maximum value at $t_0 - \theta \approx \pm n\pi, n = 0,1,2$, etc. Here ϕ is at the peak of the sinusoid, and stays high for at least a quarter cycle of the hour angle ($\approx$6–9 hr). Using this relation and proceeding as in the previous section, one obtains

$$\sigma_u|_{\rm min} = \frac{1}{\pi}\frac{\lambda}{d_{u2}}\sqrt{\frac{1}{N}\left[\frac{1+f}{f}\right]}\sigma_{\rm obs},$$
$$\sigma_v|_{\rm min} = \frac{1}{\pi}\frac{\lambda}{d_{v2}}\sqrt{\frac{1}{N}\left[\frac{1+f}{f}\right]}\sigma_{\rm obs}, \qquad (21)$$

where

$$\frac{1}{d_{u2}} = +\frac{[X\cos t_0 - (Y\sin\Lambda - Z\cos\Lambda)\sin t_0]}{R^2}\frac{1}{\sqrt{1+2k_2^2 + 4k_2\frac{\sin\Delta t/2}{\Delta t/2} + \frac{\sin\Delta t}{\Delta t}}},$$
$$\frac{1}{d_{v2}} = +\frac{[X\sin t_0 + (Y\sin\Lambda - Z\cos\Lambda)\cos t_0]}{R^2}\frac{1}{\sqrt{1+2k_2^2 + 4k_2\frac{\sin\Delta t/2}{\Delta t/2} + \frac{\sin\Delta t}{\Delta t}}},$$
$$k_2 = \frac{(Y\cos\Lambda + Z\sin\Lambda)[X\sin t_0 + (Y\sin\Lambda - Z\cos\Lambda)\cos t_0]}{\tan\delta R^2}. \qquad (22)$$

Only the final results have been written down here, since the algebra closely follows that of the previous section. Equations (18) and (21) together specify the error estimates on L_u and L_v; often only one of the two equations need be used.

Now let $d \ll c$. Then the d.c. value in Fig. 3 will be much larger than the amplitude of the sine wave, and the smallest possible values of $\phi(t)$ occur in the duration of observation centered at $t_0 - \theta \approx \pm 180°, \pm 540°$, etc., for positive values of c and at $t_0 - \theta \approx 0°, \pm 360°$, etc., for negative values of c; this simply means that Eq. (21) should be used in place of Eq. (18) for the error estimation. In the intermediate case where $d \approx c$ it becomes difficult to estimate exactly the effective baseline length for the observation. Equations (18) and (21) then offer only an approximate estimate of the errors. Table III shows that in such situations the expected σ_u and σ_v can be off by a factor of 2, on the average, from the true

values. However the qualitative form of σ_u and σ_v remains the same.

c) σ_u and σ_v at Very Low Declinations

The above formulation is not valid at very small declinations, where the tan δ in Eq. (20) blows up; Eq. (14) can no longer be used, since sin $\delta \approx 0$. In this case L_v projects only along the rotation axis of *E*arth [see Fig. 2(a)], and in Eq. (10) d depends only on l_u, c depends only on l_v as before, and θ is independent of both of them. Proceeding as in Sec. II*a* it can be shown that the errors σ_u and σ_v are of the same form as in Eq. (18), with $d_{u1} \approx R$ and $d_{v1} \approx (Y \cos \Lambda + Z \sin \Lambda)$. This particular case is not discussed in detail here as it is not likely to be encountered often in practice.

It should be emphasized here that the limits $\delta \approx 0°$ or $d \approx c$ only affect the exact estimation of the effective baseline length d_{eff}; they will not change the qualitative form of σ_u or σ_v as given in Eqs. (18) and (21).

d) Results of Simulations

Table I shows the result of model fitting four simulated datasets. The binary parameters L_u,L_v, and f, the physical baseline components X, Y, and Z, and the other parameters δ, Λ, λ, and N have been chosen at random. In each case Gaussian random noise was added to the visibilities, of rms values 0.05, 0.15, and 0.30. Comparing this with the highest possible visibility value of 1.00, the three datasets can be qualitatively classified as "good," "average," and "poor," respectively. Observations are centered at transit of the binary (i.e., $t_0 \approx 0°$), and the duration of observation is $\approx$6–9 hr.

Each box in Table I shows, for that situation, the σ_u and σ_v expected on the basis of Eq. (18) and Eq. (21), as well as those actually obtained from the simulated data (by searching for the L_u and L_v at which the χ^2 increases by 1). There is good agreement between the observed and expected rms, errors on L_u and L_v. In most cases the discrepancy is within $\approx$10%; in the last case of example 3 it is $\approx$20%. In this example Eq. (18) was used to estimate σ_v and Eq. (21) was used to estimate σ_u. It is concluded that the rms errors on the binary separations L_u and L_v are reasonably represented by the model of Sec. II.

III. ALTERNATE SOLUTIONS FOR L_u AND L_v

Consider two binary separations differing by l_u and l_v, that are much larger than the formal errors σ_u and σ_v. If the rms difference between the two expected visibility curves (as a function of hour angle t) is comparable to the rms noise on the observed visibility data, then both solutions will be statistically consistent with the same data. At first glance this might appear unlikely in a real situation, since the change in the visibility phase $\phi(t)$ is directly proportional to the departure $\sqrt{l_u^2 + \sin^2\delta l_v^2}$, and the systematic variance of the visibility is quadratically proportional to $\phi(t)$. However, the visibility varies as the cosine of $\Phi(t)$ [Eq. (1)], and changes in Φ of $\pm n2\pi$, $n = 1,2,3$, etc. drop out, and only $\phi(t)$ modulo $\pm n2\pi$ is effective in Eq. (1). Thus $\phi(t)$ can be made "small" by the proper choice of l_u and l_v (Sec. IV discusses what one implies by "small" changes in ϕ). Moreover, it can be maintained small over a duration of $\approx$6–9 hr of observation if l_u and l_v are chosen such that $t_0 - \theta \approx n\pi$, by the argument of Sec. II*b*. Under these conditions $\langle \Delta I^2 \rangle$ will be a "small" quantity, even though l_u and l_v are much larger than their rms errors σ_u and σ_v, respectively; and this is the mathematical basis of the alternate solutions.

Two quantities characterize the alternate solutions—r_a, the separation in the L_u,sin δL_v space between any two neighboring multiple solutions, and Θ_a, the direction along which they lie in this space. By substituting $t - \theta = t' \pm n\pi$ into Eq. (9) one obtains the direction that one has to follow in the L_u,L_v space to satisfy this criterion; this direction lies at angle Θ_a measured with respect to the L_u axis

$$\Theta_a = \arctan\left(\frac{X \sin t_0 + (Y \sin \Lambda - Z \cos \Lambda)\cos t_0}{X \cos t_0 - (Y \sin \Lambda - Z \cos \Lambda)\sin t_0}\right). \tag{23}$$

It is understood that the opposite direction $180° + \Theta_a$ is also valid for the alternate solutions. Along these directions a departure of $l = \sqrt{l_u^2 + \sin^2 \delta l_v^2}$ changes the visibility phase by

$$\phi(t') = (-1)^n (2\pi/\lambda) lR\,(\cos t' + k_2). \tag{24}$$

The alternate solutions occur when $\phi(t') \approx 2\pi$ or multiples of it, i.e.,

$$\frac{2\pi}{\lambda} lR\,(1 + k_2) \approx \pm 2n\pi,$$

$$\Rightarrow r_a = \frac{\lambda}{R}\left(\frac{1}{1 + k_2}\right)$$

$$\approx \frac{\lambda}{R}\,\frac{1}{1 + \tan \delta}. \tag{25}$$

Thus the first pair of alternate solutions lie at separation r_a along the azimuths Θ_a and $180° + \Theta_a$ in the L_u,sin δL_v space; the second pair lie at separation $2r_a$ along the same directions, and so on. Θ_a is simply the direction along which the physical baseline is projected in the equatorial plane at the instant t_0, i.e., at the mean hour angle for the observations. It is intuitively clear that binary separations along this direction give visibility phases that vary least with hour angle, during a finite hour angle range centered at t_0, since Φ varies approximately cosinusoidally with t in this configuration. r_a is simply the binary separation that will increase the visibility phase by 2π for the baseline projected onto the equatorial plane. By increasing the binary separation by r_a in the direction Θ_a, one jumps a fringe in the sky, or sidelobe, of the "projected" interferometer. Thus the alternate solutions can be looked upon as observations of the binary with the sidelobes of the interferometer projected onto the equatorial plane. This is only an approximate picture, since the components of the binary separation and physical baseline along the rotation axis of Earth also contribute to the phase difference ϕ.

Figure 4 illustrates the alternate solutions of example 1 in Table I, for $\sigma_{\text{obs}} = 0.05$. Figure 4(a) shows the best fit to the data at $L_u = -20.433$ mas and $L_v = +14.282$ mas; the rms errors on these are $\sigma_u = 0.035$ mas and $\sigma_v = 0.044$ mas, respectively (Table I). From Eqs. (23) and (25) r_a is computed to be 5.998 mas and Θ_a to be 48.6242°. Thus the first alternate solution is expected at $L_u = -20.433 + 3.965 = -16.468$ mas and $L_v = +14.282 + 4.501/\sin \delta = +20.647$ mas, which are quite different from the true values. This fit is shown in Fig. 4(b); it is excellent between hour angles -1 and $+1$ hr, not bad between -2 and $+2$ hr, and deteriorates rapidly outside this range. Figure 4(c)

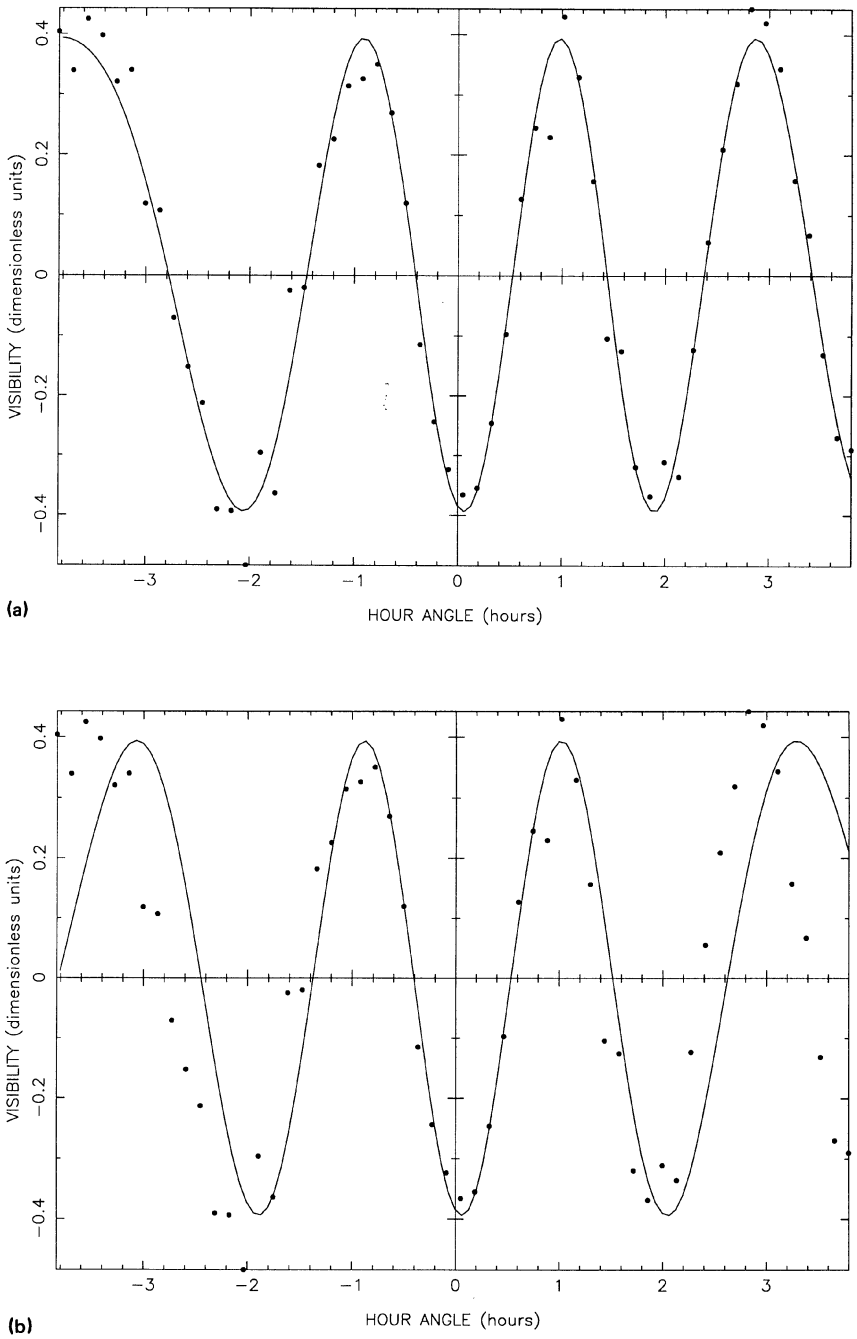

FIG. 4. Illustration of the true solution and first two pairs of alternate solutions of example 1 in Table I. The dots mark the simulated visibility data with an rms Gaussian noise $\sigma_{obs} = 0.05$, while the curve is the theoretical fit. (a) True solution a $L_u = -20.433$ mas and $L_v = +14.282$ mas; (b) and (c). The first pair of alternate solutions at $L_u = -16.468$ mas and $L_v = +20.647$ mas, and $L_u = -24.398$ mas and $L_v = +7.917$ mas, respectively. (d), (e) The second pair of alternate solutions at $L_u = -12.503$ mas and $L_v = 27.013$ mas, and $L_u = -28.363$ mas and $L_v = 1.551$ mas, respectively. With more noisy data solutions (b) and (c) could be indistinguishable from solution (a) if the duration of observation Δt was a couple of hours around $t_0 \approx 0$.

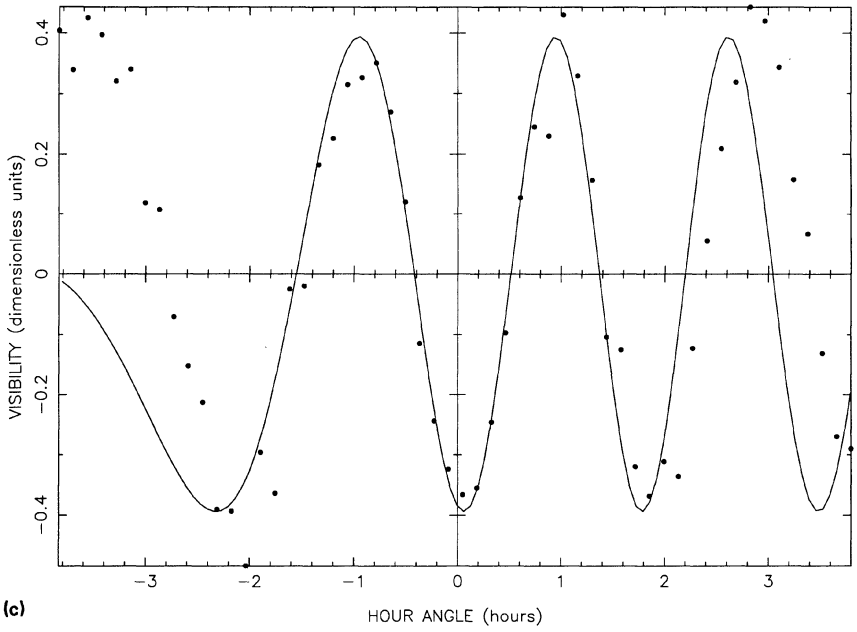

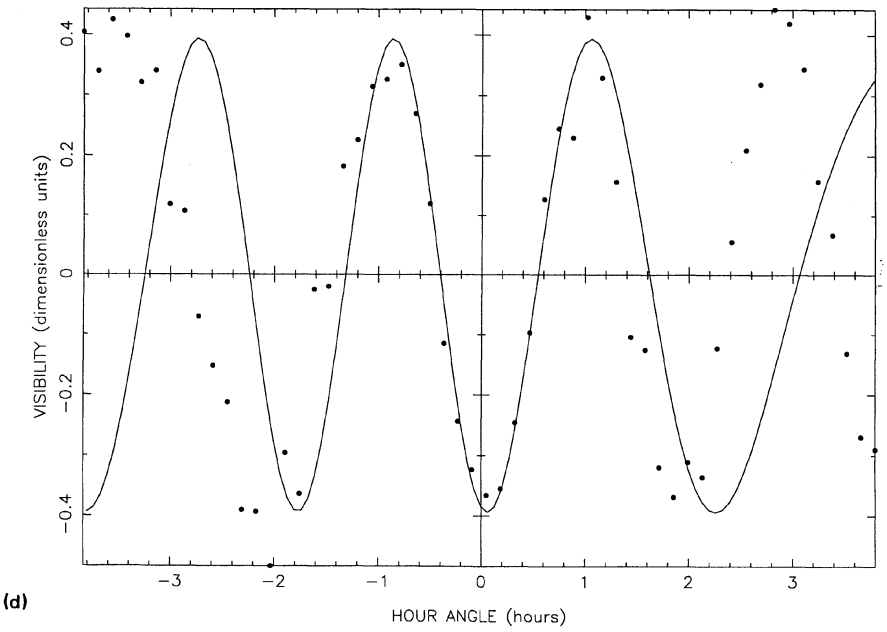

FIG. 4. (continued)

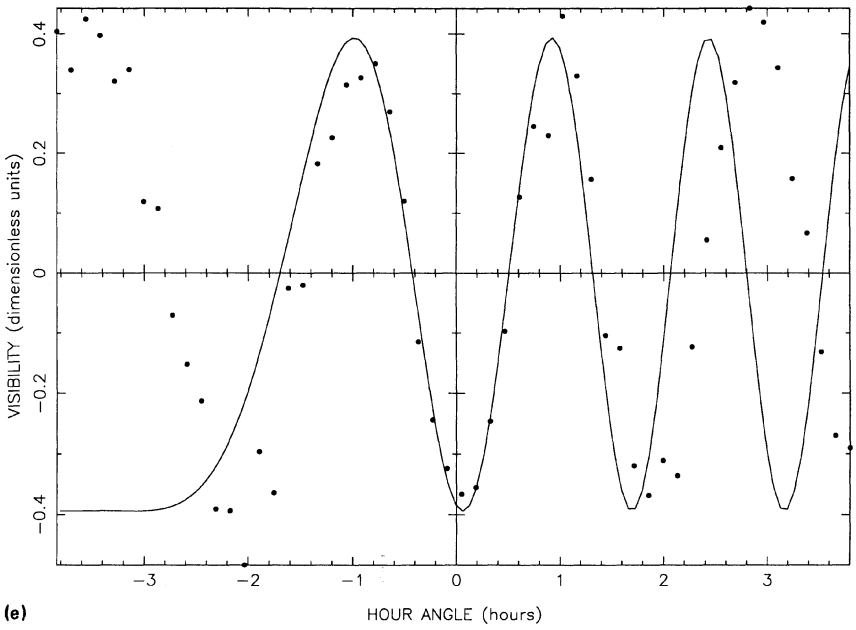

FIG. 4. (continued)

shows the first alternate solution on the other side of the true solution, i.e., at $L_u = -20.433 - 3.965 = -24.398$ mas and $L_v = +14.282 - 4.501/\sin\delta = +7.917$ mas; it shows the same qualitative features as Fig. 4(b). It is obvious that at $\sigma_{\rm obs} = 0.05$ these alternate solutions can be ruled out based on χ^2 alone; however, they become serious candidates if, for example, the binary was observed only between hour angles -1 and $+1$; or if it was observed between -2 and $+2$ hr and the visibility data was more noisy.

Figure 4(d) shows the second alternate solution at $L_u = -20.433 + 7.930 = -12.503$ mas and $L_v = +14.282 + 9.002/\sin\delta = 27.013$ mas; and Fig. 4(e) shows the corresponding solution on the other side of the true solution. For these solutions the fit is still plausible between -1 and $+1$ hr, though it is entirely unacceptable outside this range. Thus even the second alternate solutions have to be considered seriously if the duration of observation is very small and is centered at transit, and the data is more noisy.

The same qualitative behavior is found in the rest of the examples of Table I. It is thus concluded that alternate solutions are indeed found at separations $\approx r_a$ in the directions Θ_a and $\Theta_a + 180°$.

The systematic variance $\langle \Delta I^2 \rangle_a$ at any of the alternate solutions is difficult to estimate accurately; however, an order of magnitude estimate is certainly possible. At the alternate solution the change in visibility phase ϕ is obtained by dropping the constant part in Eq. (24), since it is $\approx \pm n2\pi$, and retaining the first few terms in the Taylor expansion of $\cos t'$. Then

$$\phi(t') \approx (-1)^n \frac{2\pi}{\lambda} lR \left(-\frac{t'^2}{2} + \frac{t'^4}{24} - \ldots \right). \qquad (26)$$

Even this residual phase of Eq. (26) could have a d.c. value, since it is difficult to estimate exactly at what l is $\phi(t)$ modulo 2π a minimum, on the average, in the duration of observation. So the systematic variance at the alternate solutions can be defined as

$$\langle \Delta I^2 \rangle_a = \langle \Delta I^2 \rangle - \langle \Delta I \rangle^2,$$
$$= \frac{1}{90}\left(\frac{2\pi}{\lambda}\right)^2 \left(\frac{f}{1+f}\right)^2 l^2 R^2 \left(\frac{\Delta t}{2}\right)^4 \left[1 - \frac{1}{7}\left(\frac{\Delta t}{2}\right)^2 + \frac{1}{180}\left(\frac{\Delta t}{2}\right)^4 - \ldots\right]. \qquad (27)$$

Equation (27) is expected to provide only a ball-park estimate due to the approximate derivation. The analysis of this section closely follows that of Sec. II*b*.

Table II compares the expected $\langle \Delta I^2 \rangle_a$ with the observed residuals for the alternate solutions in Table I. $\sigma_{\rm obs}$ is fixed at 0.05 since at higher values the alternate solutions can only be expected to become more acceptable. The observed and expected rms deviations of the data from the model agree to within a factor of 3, the discrepancy being larger for the more distant alternate solutions. We conclude that Eqs. (23) and (25) represent, to a good order of accuracy, the parameters of alternate solutions.

IV. DISCUSSION

A number of approximations have gone into the derivations above. First, it was assumed that ϕ is a small quantity, from which Eq. (11) followed. From Eq. (9) it is clear that the maximum value ϕ can attain is $|d| + |c|$, which is always less than $(2\pi/\lambda) L_g L_b$, where $L_g = \sqrt{X^2 + Y^2 + Z^2}$ is the length of the physical baseline, and $L_b = \sqrt{L_u^2 + L_v^2}$ is the binary separation in the plane of the sky. This can be put as

$$\phi|_{\rm max} = L_b\,({\rm mas}) \left(\frac{L_g(m)}{18}\right) \left(\frac{\lambda(\mu)}{0.55}\right)^{-1} {\rm radians}, \qquad (28)$$

where L_b is measured in milliarcseconds, L_g in meters and λ in microns. Ideally $\phi|_{\rm max}$ should be a small quantity ($\ll 1$ radian) for the validity of the above analysis. For large durations of observation this condition is violated, first at the edges of the observed range of hour angle, and later progres-

sively towards the center of the hour angle range. For example, this condition is violated in example 3 of Table I, which explains the relatively higher discrepancy between simulated and observed σ_u and σ_v.

Second, it was assumed that the visibility varies by at least one cycle in the observed hour angle range, so that one could neglect terms of the type $\sin[2\Phi(t)]$ and $\cos[2\Phi(t)]$ in Eq. (12). The accuracy of the formulas in this article is suspect when this condition is no longer met. However, this condition is almost mandatory from an observational point of view also, because of the problem of multiple solutions. Therefore this assumption is very reasonable.

The third assumption was that the observed range of hour angle be around 6–9 hr. This is strictly not necessary, and mainly helps to understand the derivations in this article. If this condition were met, then it is easy to see along which direction the systematic variance $\langle \Delta I^2 \rangle$ changes fastest, or slowest, since the observed hour angle range would straddle either the peak, or the null, of the phase error curve ϕ in Fig. 3. If the range of hour angle is very large, then the systematic variance would increase at the same rate no matter along which direction the parameters were changed, i.e., the error ellipse would become a circle in the l_u,sin δl_v space. But the errors σ_u and σ_v obtained from Eqs. (18) and (21) will still be representative.

At very low declinations δ and latitudes Λ the geometry of the problem changes significantly, in the sense that there is hardly any projection of either the Y component of the physical baseline, or the L_v component of the binary separation, onto the equatorial plane. However the X component of the physical baseline, and the L_u component of the binary separation continue to project onto the equatorial plane; thus the principles of derivation of this article continue to hold.

The most critical approximation in this article is the assumption that $t_0 - \theta \approx \pm 90°, \pm 270°, \ldots$ in Sec. II*a* and that $t_0 - \theta \approx 0°, \pm 180°, \ldots$ in Sec. II*b*. In principle one should use the approximation $d\cos(t_0 - \theta) + c \approx 0$ to obtain the smallest values of ϕ in the observed range of hour angle, as shown in Fig. 3, and then solve for $\langle \Delta I^2 \rangle$. Then the analytic derivation of σ_u and σ_v becomes difficult. Table I shows that the above approximations are reasonably accurate, on the average, in varied situations. In practice it is sufficient to predict the random errors σ_u and σ_v approximately, since any real data will also have systematic errors as shown in Table III.

Table III presents the results of applying the theory of Sec. II to real data from the Mark III Optical Interferometer at Mount Wilson. The data was obtained in the year 1989. Observed and expected σ_u and σ_v are shown for four different nights of observations of the binary star α Andromeda, using three different baseline lengths. Columns 2, 3, and 4 contain the X, Y, and Z components of the physical baseline in meters. Columns 5 and 6 contain the central hour angle t_0 and the total duration of observation Δt in hours. Columns 7 and 8 contain the effective beamwidths λ / d_{u2} along the right ascension and λ / d_{v1} along declination respectively in milliarcseconds [Eq. (21) is used for σ_u and Eq. (18) for σ_v]. Column 9 contains the total number of visibilities observed each night, and column 10 contains the observed rms noise σ_{obs} on the visibility squared data. At the Mark III the square of the visibility is used for data analysis, instead of the visibility itself, as it is an unbiased observable (Colavita 1985). Equation (13) can still be used by replacing $f/(1+f)$ by $2f/(1+f)^2$ [this follows directly from Eq. (1)]. Thus only this change needs to be made in Eqs. (18) and (21). Columns 11 and 12 have the expected and observed σ_u while columns 13 and 14 contain the expected and observed σ_v, respectively, all in mas. Table III(a) refers to data obtained at a wavelength of 0.8 μm, while Table III(b) refers to data at 0.55 μm. The expected rms errors are ≈ 2.5 times smaller, on the average, than the observed ones at $\lambda = 0.8$ μm, while they are ≈ 1.8 times smaller at $\lambda = 0.55$ μm. In two cases the disagreement factors are 4 and 3, respectively. Since the Mark III has essentially a north–south baseline, the star sees mostly a V component of the projected baseline during the observations. This therefore is a case where $|d| \approx |c|$, which could explain part of the above discrepancy. Part of it is probably due to systematic errors that appear to affect the data. For example, consider the data of August 31 and September 2. The former has almost twice the number of data points (34 against 19), and marginally lower σ_{obs} at 0.8 μm (1.6% against 1.9%). So one expects the observed errors on August 31 to be $\approx 50\%$ lower than the errors on September 2; but the observed σ_u is higher in the former data, while the observed σ_v is the same in both data. At 0.55 μm the observed σ_u and σ_v are the same on both days, whereas one expects the same $\approx 50\%$ difference. This behavior cannot be explained solely by random errors. A deeper analysis of these effects is beyond the scope of this article.

Figure 5 illustrates the alternate solution found in the 0.8 μm data obtained on 7 October 1989, with the Mark III. Figure 5(a) shows the fit at the true solution of $L_u = -11.84$ mas and $L_v = -6.79$ mas. r_a for this night's baseline configuration is computed from Eq. (25) to be 2.554 mas and Θ_a is computed from Eq. (23) to be $-91.077°$. Figure 5(b) shows the fit at the first alternate solution of $L_u = -11.99$ mas and $L_v = 12.21$ mas, while Fig. 5(c) shows the fit at the corresponding alternate solution of $L_u = -11.66$ mas and $L_v = -1.34$ mas, on the other side of the true solution. The χ^2 per degree of freedom of the three fits are 0.65, 0.83, and 0.90, respectively. With seven independent degrees of freedom in each figure, the alternate solutions can be rejected on the basis of χ^2 alone. However, the χ^2 of Fig. 5(b) is not too different from that of the true solution, and the two might have been indistinguishable if the rms noise on the observed visibilities had been a bit higher. A lot of the difference in the three fits occurs in the first one hour of the observation. Had the observation begun an hour later, the three solutions might have been inseparable.

The results of Sec. III suggest an observational method of resolving the alternate solutions (apart from obtaining data of very good quality!). If the binary star is observed on two baselines with significantly different orientations, then the alternate solutions for each baseline will lie along different straight lines in the L_u and sin δL_v space, spaced by different intervals, as per Eqs. (23) and (25). Only the true solution will be common to the two baselines (this suggestion is due to Michael Shao).

To obtain errors in L_u and L_v that are comparable, the effective baseline length d_{eff} must have comparable projections along the two axis. At optical wavelengths observations are generally restricted to high elevations of the star, due to the atmospheric absorption. Thus Earth rotation will not be efficient in rotating a given physical baseline in the U,

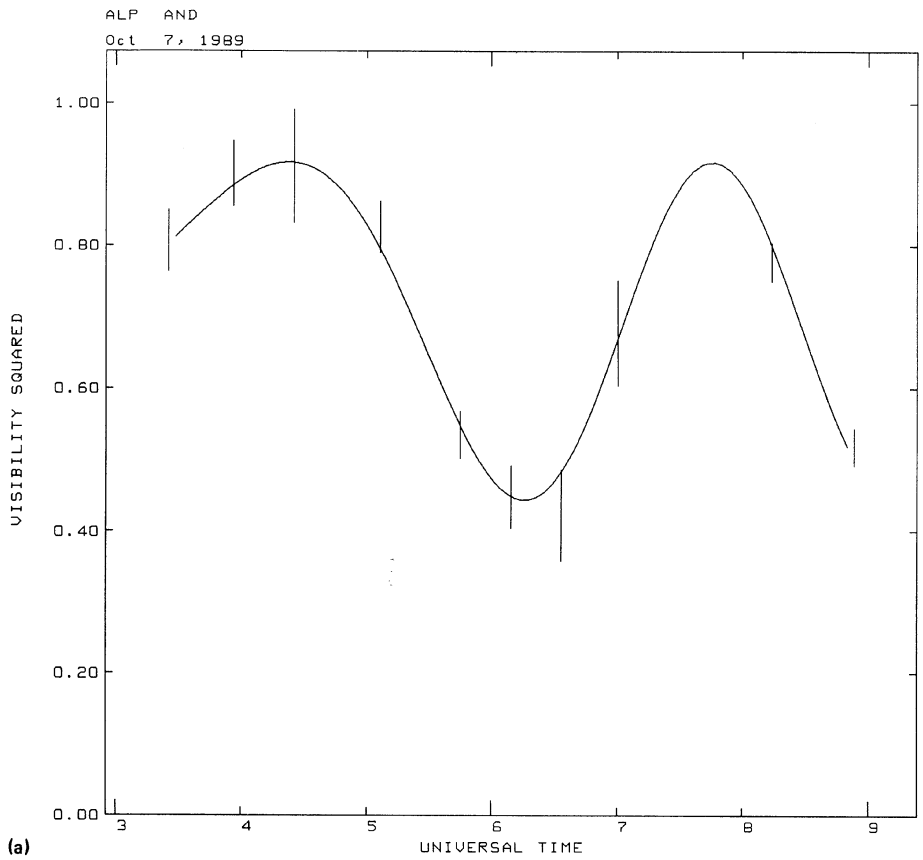

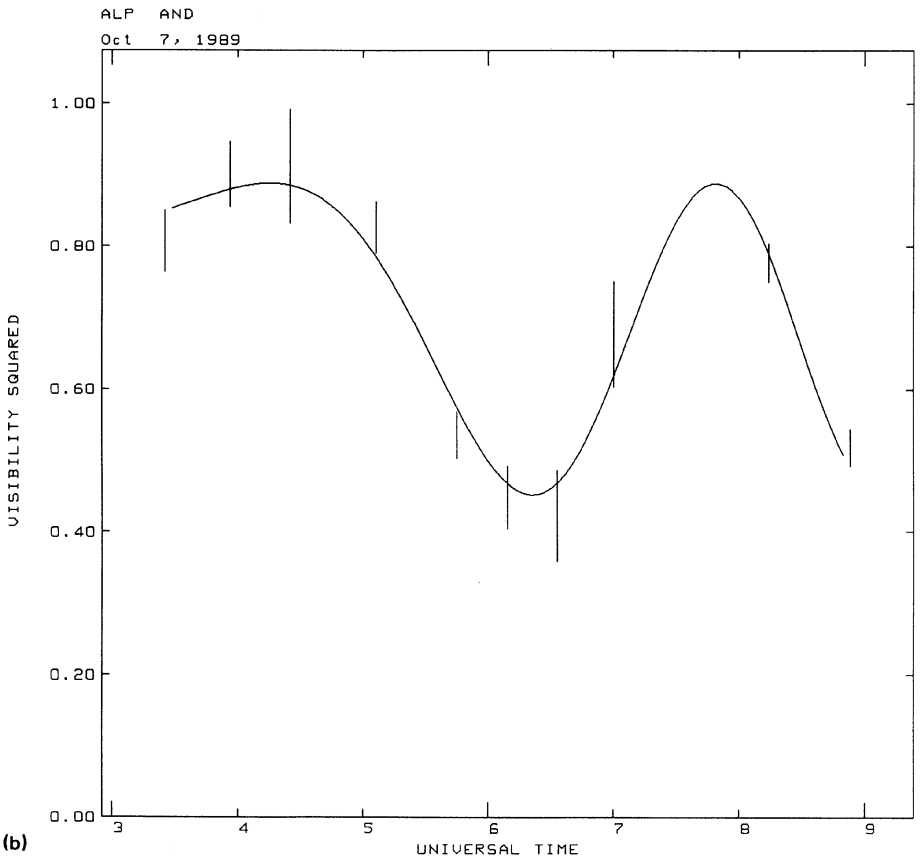

FIG. 5. Solutions of binary separation of the star α Andromeda in data of 7 October 1989. (a) The true solution at $L_u = -11.84$ mas and $L_v = -6.79$ mas. (b) and (c) The first pair of alternate solution at $L_u = -11.99$ mas and $L_v = -12.21$ mas, and $L_u = -11.66$ mas and $L_v = -1.34$ mas, respectively. The χ^2 per degree of freedom of the three fits are 0.65, 0.83, and 0.90, respectively. Note that the square of the visibility has been used to analyze the data. The three solutions would have been indistinguishable at higher noise levels.

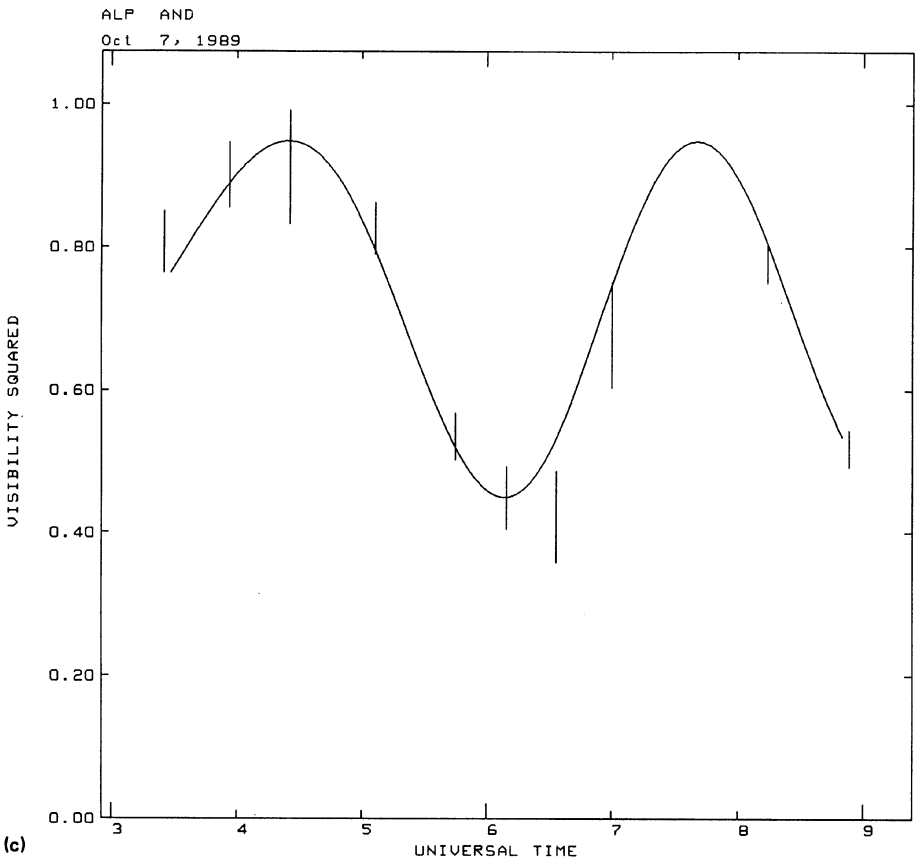

FIG. 5. (continued)

V plane. It is therefore necessary to have both an east–west and a north–south component of the physical baseline to start with (this implication is intuitively obvious).

I wish to thank Michael Shao, Dave Mozurkewich, Mark Colavita, and Ken Johnston for useful discussions, and Xiao-Pei Pan for the data of Table III.

REFERENCES

Colavita, M. M. (1985). Ph.D. thesis, Massachusetts Institute of Technology.
Labeyrie, A. (1975). Astrophys. J. Lett. **196**, L71.
Shao, M., Colavita, M. M., Hines, B. E., Staelin, D. H., Hutter, D. J., Johnston, K. J., Mozurkewich, D., Simon, R. S., Hershey, J. L., Hughes, J. A., and Kaplan, G. H. (1988). Astron. Astrophys. **193**, 357.
Thompson, A. R., Moran, J. M., and Swenson, G. W. (1986). *Interferometry and Synthesis in Radio Astronomy* (Wiley, New York).